SECURITY CLASSIFICATION OF THIS PAGE

REPORT DOCUMENTATION PAGE

1a. REPORT SECURITY CLASSIFICATION: Unclassifi	1b. RESTRICTIVE MARKINGS
2a. SECURITY CLA:	3. DISTRIBUTION/AVAILABILITY OF REPORT: Approved for Public Release Distribution Unlimited
2b. DECLASSIFICA: **AD-A201 350**	
4. PERFORMING O: MDC K0171	5. MONITORING ORGANIZATION REPORT NUMBER(S): AFOSR-TR- 88-1178
6a. NAME OF PERFORMING ORGANIZATION: McDonnell Douglas Corp. Douglas Aircraft Company	6b. OFFICE SYMBOL (If applicable): DAC
7a. NAME OF MONITORING ORGANIZATION: Air Force Office of Scientific Research	
6c. ADDRESS (City, State and ZIP Code): 3855 Lakewood Boulevard Long Beach, CA 90846	7b. ADDRESS (City, State and ZIP Code): Bolling AFB Washington, DC 20332 BR141C
8a. NAME OF FUNDING/SPONSORING ORGANIZATION: AIR FORCE OFFICE OF SCIENTIFIC RESEARCH	8b. OFFICE SYMBOL (If applicable): AFOSR/NA
9. PROCUREMENT INSTRUMENT IDENTIFICATION NUMBER: F49620-84-C-0007	
8c. ADDRESS (City, State and ZIP Code): Building 410 Bolling AFB, DC 20332	10. SOURCE OF FUNDING NOS.

PROGRAM ELEMENT NO.	PROJECT NO.	TASK NO.	WORK UNIT NO.
61102F	2307	A4	

11. TITLE (Include Security Classification): THE BIRTH OF OPEN SEPARATION ON A PROLATE SPHEROID (Unclassified)

12. PERSONAL AUTHOR(S): Tuncer Cebeci Wenhan Su

13a. TYPE OF REPORT	13b. TIME COVERED	14. DATE OF REPORT (Yr., Mo., Day)	15. PAGE COUNT
~~Technical~~ FINAL	FROM 3/86 TO 9/88	1988, September	29

16. SUPPLEMENTARY NOTATION

17. COSATI CODES		
FIELD	GROUP	SUB. GR.

18. SUBJECT TERMS (Continue on reverse if necessary and identify by block number): Fluid Mechanics, Boundary Layers, Bodies of Revolution, Crossflow, Singularity, Three-Dimensional Flows, ~~Separation~~

19. ABSTRACT (Continue on reverse if necessary and identify by block number)

Results are presented to describe the laminar flow patterns around a prolate spheroid at angles of attack of 1, 2, 3, and 30 degrees and complement those obtained previously at 6 degrees. They were obtained by solving three-dimensional boundary-layer equations with a combination of standard and characteristic box methods and with a stability criterion to ensure numerical accuracy. Emphasis is placed on the nature of separation which, in agreement with experiment but contrary to some theoretical claims, is shown to be open for all angles of attack and to be coincident with a particular skin friction line.

20. DISTRIBUTION/AVAILABILITY OF ABSTRACT	21. ABSTRACT SECURITY CLASSIFICATION
UNCLASSIFIED/UNLIMITED ☒ SAME AS RPT. ☐ OTIC USERS ☐	Unclassified

22a. NAME OF RESPONSIBLE INDIVIDUAL	22b. TELEPHONE NUMBER (Include Area Code)	22c. OFFICE SYMBOL
~~Dr. James D. Wilson~~ Capt. Henry Helin USAF	202/767-4935	AFOSR/NA

DD FORM 1473, 83 APR EDITION OF 1 JAN 73 IS OBSOLETE. Unclassified

SECURITY CLASSIFICATION OF THIS PAGE

88

Report No. MDC K0171

AFOSR-TR- 88-1178

THE BIRTH OF OPEN SEPARATION ON A PROLATE SPHEROID

by

Tuncer Cebeci

Aerodynamics Research and Technology
Douglas Aircraft Company

and

Wenhan Su

Aerospace Engineering Department,
California State University, Long Beach

September 1988

This work was completed under
Air Force Office of Scientific Research
Contract F49620-84-C-0007

ABSTRACT

Results are presented to describe the laminar flow patterns around a prolate spheroid at angles of attack of 1, 2, 3, and 30 degrees and complement those obtained previously at 6 degrees. They were obtained by solving three-dimensional boundary-layer equations with a combination of standard and characteristic box methods and with a stability criterion to ensure numerical accuracy. Emphasis is placed on the nature of separation which, in agreement with experiment but contrary to some theoretical claims, is shown to be open for all angles of attack and to be coincident with a particular skin friction line.

TABLE OF CONTENTS

LIST OF FIGURES

1.0 INTRODUCTION

Prediction of separation patterns on three-dimensional bodies is important in engineering practice and a complete solution to the problem requires either the solution of the Navier-Stokes equations or of inviscid flow and boundary-layer equations with interaction between the two. The calculations are difficult and remain to be performed satisfactorily. In the meantime, attention has been directed to the solution of model problems where the external velocity distribution has been determined from an analytic expression based on a simple body shape with three-dimensional boundary-layer equations solved numerically. It should not be expected that the measurements of, for example, Han and Patel (1975), Meier and Kreplin (1980), Meier, Kreplin and Vollmers (1983), and Costis, Polen, Hoang and Telionis (1988), will agree in detail with the solutions of the model problem but the latter allows the development of essential numerical techniques which pave the way for the more complete solution referred to above. It can be expected that the model problem will emphasize the sensitivity of calculation methods in the region of separation and allow the nature of flow separation to be identified; it is this aspect which is the major consideration of this report. Reference should be made to the contribution of Williams (1977) for a discussion of the various definitions of boundary-layer separation in three-dimensional flows.

An important aspect of the subject was considered by Lighthill (1963) who discussed the nature of separation in three-dimensional steady laminar flows. He postulated that three-dimensional separation corresponds to a skin-friction line which is at odds with the earlier suggestion of Maskell (1955) who proposed that separation is an envelope of limiting streamlines. The argument has continued in a series of reports where, for example, Wang (1975) and Cebeci et al. (1981) have sided with Maskell and more recently Cebeci and Su (1988) reported calculations which are consistent with Lighthill's view. These recent calculations were performed with a numerical scheme which involved systematic adjustment of the grid according to a numerical stability criterion which had been subjected to careful evaluation in relation to an extensive range of steady and unsteady flow problems. They corresponded to the laminar flow around a prolate spheroid of thickness t = 1/4 at 6 degrees angle of attack and, as shown in Fig. 1, there is a region of positive crossflow, followed by a substantial region of negative crossflow, a separation line and two terminal

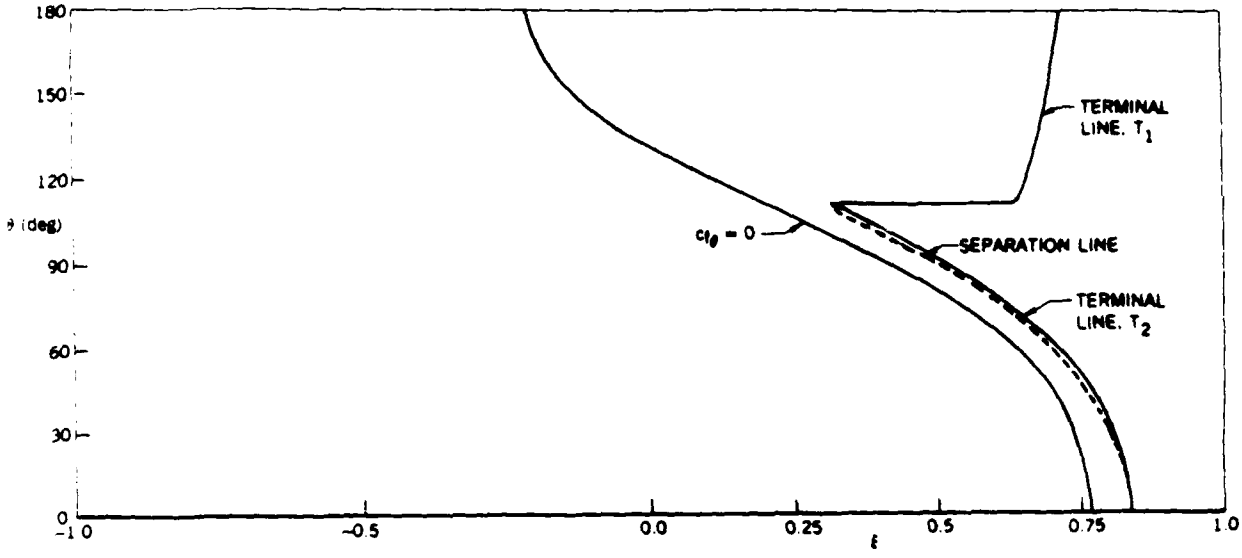

Figure 1. Flow regions for $\alpha = 6°$, according to Cebeci and Su (1988).

lines beyond which solutions of the boundary-layer equations could not be obtained. Of particular note was the separation line which did not extend from the leeward to the windward side implying open separation and is in contrast to the earlier findings of Wang (1975) and Cebeci et al. (1981).

The nature of the problem may be explained in terms of the comprehensive examination of the influence of angle of attack by Wang (1976) who presented a figure which showed the sequence of separation patterns on the prolate spheroid for a range of angles of attack. It showed that (Fig. 2a) the flow separates at a fixed parallel for zero incidence, that a small increase of incidence ($\alpha = 3°$) tilts the separation line slightly and that separation is preceded by a small region of weak reversal of the circumferential flow (Fig. 2b). As the incidence angle further increases ($\alpha = 6°$, Fig. 2c), the leeside separation point moves rearward rather than forward so that the separation line is bent as shown in an enlarged view (Fig. 3a). The upper branch AC inclines rearward, whereas the lower branch CD inclines forward. Meanwhile, the reversal of the circumferential flow starts ahead of the midbody on the leeside (see Fig. 2c). At higher incidence, the separation line breaks so that the lower branch CD extends forward to become an open separation line, as shown in Fig. 2d and enlarged in Fig. 3b. The change from a closed separation at low incidence to an open separation at higher incidence thus evolves gradually and it is difficult to identify a particular incidence at which this change takes

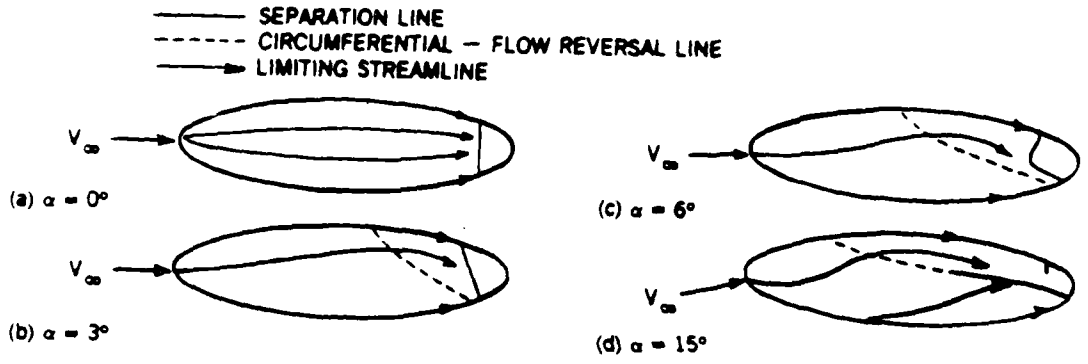

Figure 2. Sequence of flow separation on a prolate spheroid, according to Wang (1976).

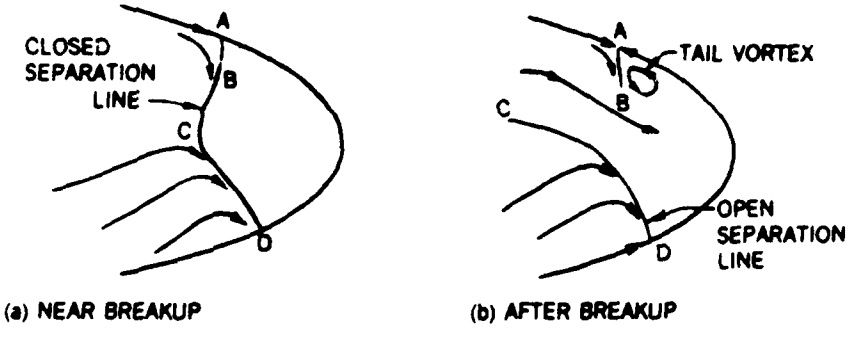

Figure 3. Initiation of open separation on a prolate spheroid a $\alpha = 6°$, according to Wang (1976).

place. Even for 6° incidence (Fig. 2c and Fig. 3a), it is difficult to say whether the separation line is closed in the section BC.

The description of the previous paragraph is in some contrast to the measurements of Meier et al. (1983) and, even though exact concurrence with calculations based on specified pressure distributions is not possible, agreement with general features of the flow might be expected. Figure 4 shows the separation

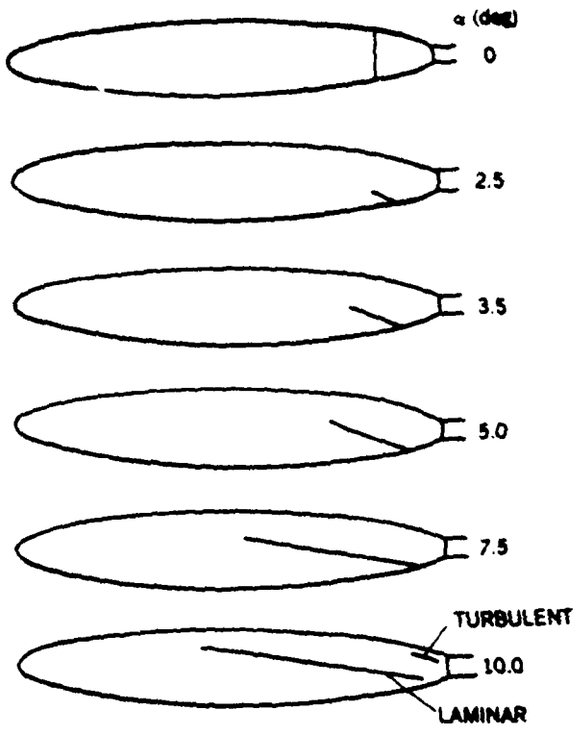

Figure 4. Separation lines derived from oil flow patterns of laminar boundary layers, according to Meier et al. (1983).

line detected by Meier et al. from their observation of the bifurcation of oil flow patterns and it is evident that the separation is open for all angles of attack greater than zero and in general agreement with the calculations of Cebeci and Su at 6 degrees. A similar conclusion was reached by Costis et al. who used dyes and particles to visualize the flow close to the surface of a prolate spheroid of fineness ratio four, rather than a ratio of six as in the results of Wang, Meier et al. and Cebeci and Su. The visualization patterns show that their separation was open for angles of attack from 6 to 30 degrees and less readily defined at 3 degrees.

Thus the purpose of the present report is to present calculations performed with the procedure used by Cebeci and Su (1988) and to determine if the differences between their results at $\alpha = 6°$ and the description of the previous paragraph also exist at other angles of incidence. At the same time, the results are examined in terms of the postulations of Lighthill and Maskell to determine the nature of the separation line. To achieve these purposes, results are presented for incidence angles of 1, 2, 3, and 30 degrees.

The following section provides a brief description of the method used to solve the three-dimensional boundary-layer equations and emphasizes the special precautions taken in the vicinity of separation. The results are presented in Section 3, which discusses them in the context of the previous studies referred to above. The report ends with a summary of the more important conclusions.

2.0 CALCULATION METHOD

The calculation method used by Cebeci and Su (1988) considers the conservation equations for mass and for x- and θ-momentum in curvilinear orthogonal coordinates and obtains their solution by a finite-difference method based on Keller's box scheme for a prolate spheroid defined by

$$\left(\frac{x}{a}\right)^2 + \left(\frac{r_o}{b}\right)^2 = 1 \tag{1}$$

subject to an external velocity distribution given by the inviscid flow theory. To avoid the singularity at the nose ξ ($\equiv x/a$) = -1, in a region $-1 \leq \xi \leq \xi_0$, they used the procedure of Cebeci et al. (1980) which employs transformations that allow the boundary-layer equations to be solved without numerical difficulties. For $\xi > \xi_0$, they used two different versions of the box scheme depending on the complexity of the flowfield. In regions of positive crossflow velocity, they used the standard-box scheme and the characteristic box scheme in regions of negative crossflow velocity.

The accuracy of the calculations performed with the standard-box method is well established and that of the characteristic-box method was examined by Cebeci and Su for regions of positive crossflow and was shown to be equally satisfactory. In regions of negative crossflow and in the vicinity of the separation line, however, the results depended upon the finite-difference grid in a way which necessitated an intelligent procedure for grid spacing. To discuss this point further, let us consider the net shown in Fig. 5 at a distance y from the surface and assume that the solutions with the characteristic box scheme originate on the leeward line of symmetry and march towards the windward line of symmetry. The symbol x denotes the location where the solution is known and the symbol o denotes the location where the solution is to be found. The backward characteristic from point P is in the local streamline direction and intersects the ξ_{i-1} line at E when there is a positive crossflow velocity and at F when the crossflow velocity is negative. Since the characteristic box computes the region EFP, which is known as the domain of dependence of point P, it ensures that the domain of stable computations can be determined a priori and this is achieved by determining the ratio $\beta(\equiv\Delta\theta_1/\Delta\theta)$ which is also equal to $(w/u)(h_1/h_2)(\Delta\xi/\Delta\theta)$ and requiring that it remains small during the calculations: Cebeci and Su (1988) refer to this requirement as the

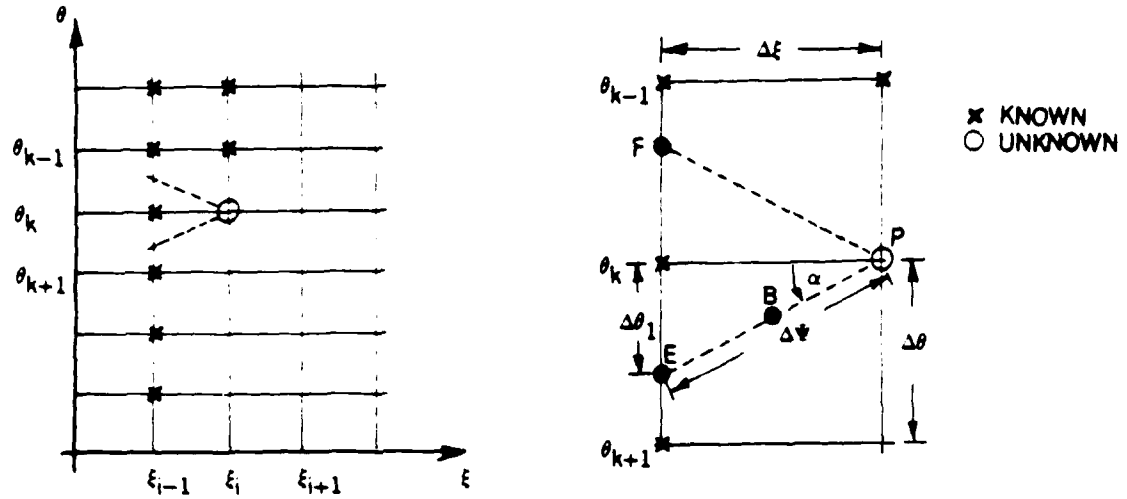

Figure 5. Finite-difference notation for the characteristic-box scheme: o, unknowns, x known.

stability criterion of the characteristic box scheme since it characterizes the flow angle and, therefore, the grid-interval required to ensure that the zones of dependence and influences are properly represented.

3.0 RESULTS

As in the study of Cebeci and Su (1988), the calculations for a given angle of attack were performed by identifying three separate regions on the body. In the region upstream of the line of zero c_{f_θ} (Region A), all u- and w-velocities are positive; in the region between this line and the two terminal lines 1 and 2 (Region B), u is positive and w is negative near the surface; and in the region downstream and between the two terminal lines (Region C) u and w are negative near the surface and positive away from the surface. The numerical calculations in Region A made use of the regular box scheme with comparatively large step sizes in the streamwise direction ξ and those in Region B made use of the characteristic box scheme with a great deal of attention was paid to the choice of the net in the circumferential and streamwise directions. Again, three subregions were identified to perform the calculations. The first subregion started at ξ_A where the w-velocity became negative and extended to ξ_p where the streamwise wall shear $(\partial u/\partial y)_w$ first vanished. The second and third subregions began at the first separation point ξ_p and were bounded by the leeward line of symmetry, the terminal line 1, the windward line of symmetry and terminal line 2.

Following the routine calculations in Region A, the calculations in Region B were started on the windward line of symmetry and continued towards the leeward line of symmetry with the standard box scheme where w is positive and the characteristic box scheme where w is negative. The step lengths in the circumferential and streamwise directions were chosen to satisfy the stability parameter β. A typical streamwise grid for uniform circumferential grid of $\Delta\theta = 2.5$ is shown in Table 1 for $\alpha = 1$, 2 and 3 degrees.

The previous study of Cebeci and Su (1988) for $\alpha = 6°$ showed that the choice of step lengths in region B was very important to the accuracy and the stability of the solutions. If they were not chosen properly, the solutions oscillated and sometimes led to breakdown of the calculations. The severity of the oscillations depended on the magnitude of the flow reversal and, when it was small, so were the oscillations. In regions close to the flow separation line, however, the solutions became more sensitive to the criterion set by the β-parameter and required that the value of β remained relatively small. A precise identification of the first (ξ_p, θ_p) location on the body where

Table 1. Axial step lengths for $\Delta\theta$ = 2.5 degrees

α = 1°		α = 2°		α = 3°	
ξ	$\Delta\xi \times 10^2$	ξ	$\Delta\xi \times 10^2$	ξ	$\Delta\xi \times 10^2$
0.0000-0.51	1.0	0.0000-0.430	1.0	0.000-0.430	1.0
0.5100-0.60	0.5	0.4300-0.550	0.5	0.430-0.500	0.5
0.6000-0.61	0.25	0.5500-0.590	0.25	0.500-0.545	0.25
0.6100-0.62	0.125	0.5900-0.606	0.10	0.545-0.560	0.10
0.6200-0.625	0.1	0.6060-0.608	0.05	0.560-0.572	0.05
0.6250-0.630	0.05	0.6080-0.6095	0.025	0.572-0.586	0.025
0.6300-0.6355	0.025	0.6095-0.6110	0.01	0.586-0.611	0.05
0.6355-0.6380	0.01	0.6110-0.6120	0.025	0.611-0.640	0.1
0.6380-0.6410	0.025	0.6120-0.6140	0.05	ξ > 0.640	0.125
0.6410-0.6440	0.05	0.6140-0.630	0.10		
0.6440-0.6500	0.1	ξ > 0.630	0.25		
0.6500-0.6550	0.125				
ξ > 0.6550	0.25				

the streamwise wall shear f''_w vanished and where g''_w was negative was very important in the calculations since that point corresponded to the definition of the open flow separation line on the prolate spheroid.

In view of the experience gained in computing α = 6° case, our studies were conducted with step lengths chosen to satisfy the stability parameter β (see Table 1) and the solutions were examined to ensure that they were smooth and free of oscillations. The grids used to compute the flow at α = 1, 2 and 3 degrees were essentially the same. For this reason, the details of the procedure are discussed for α = 3 and the remaining two will be summarized.

For α = 3°, the flow reversal in the circumferential flow direction takes place at ξ_A = 0.08 and the boundary of the line c_{f_θ} = 0 varies with ξ as shown in Fig. 6. The first ξ-location where the streamwise wall shear parameter

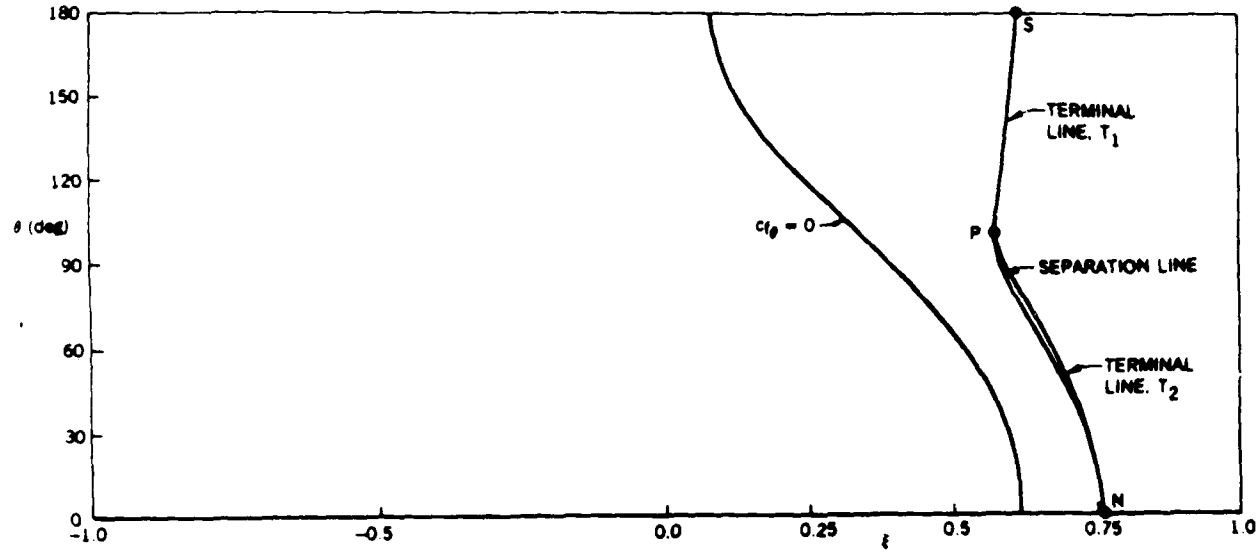

Figure 6. Flow regions for $\alpha = 3°$.

f''_w vanishes occurs at $\xi = 0.57375$, $\theta_p = 100°$. Figure 7 shows the variation of f''_w with ξ and θ, for several values of θ and ξ, and we note that f''_w vanishes at $\xi_N = 0.765$ on the windward line of symmetry ($\theta = 0$), and moves upstream with increasing θ until 100° where $\xi = 0.57375$. For values of θ greater than $\theta = 100°$, the ξ-location where f''_w is zero increases to $\xi = 0.595$ for $\theta = 140°$ and to $\xi = 0.617$ for $\theta = 180°$. The variation of f''_w with θ for given ξ-locations on the body is shown in Fig. 7b which indicates that, for values of $\xi < 0.57375$, the streamwise wall shear decreases monotonically with increasing θ up to a certain ξ-location after which it begins to increase. A sharp decrease in its magnitude takes place at $\xi = 0.57375$ for $\theta = 100°$ where, after a steep decrease in f''_w, it shows a rather sharp increase. We note from the behavior of f''_w at this angle of attack, and those at lower angles, that this rapid decrease of f''_w at a certain ξ and θ values is much less than those computed at higher angles of attack, i.e. $\alpha = 6°$. As a result, the calculations were easier to perform at the lower angles.

We see from Fig. 7, that the computed wall shear values are smooth and finite and free of oscillations. The results of Fig. 8 support this conclusion in that the magnitude of the stability parameter β is shown to be small in the circumferential direction at various ξ-locations on the body.

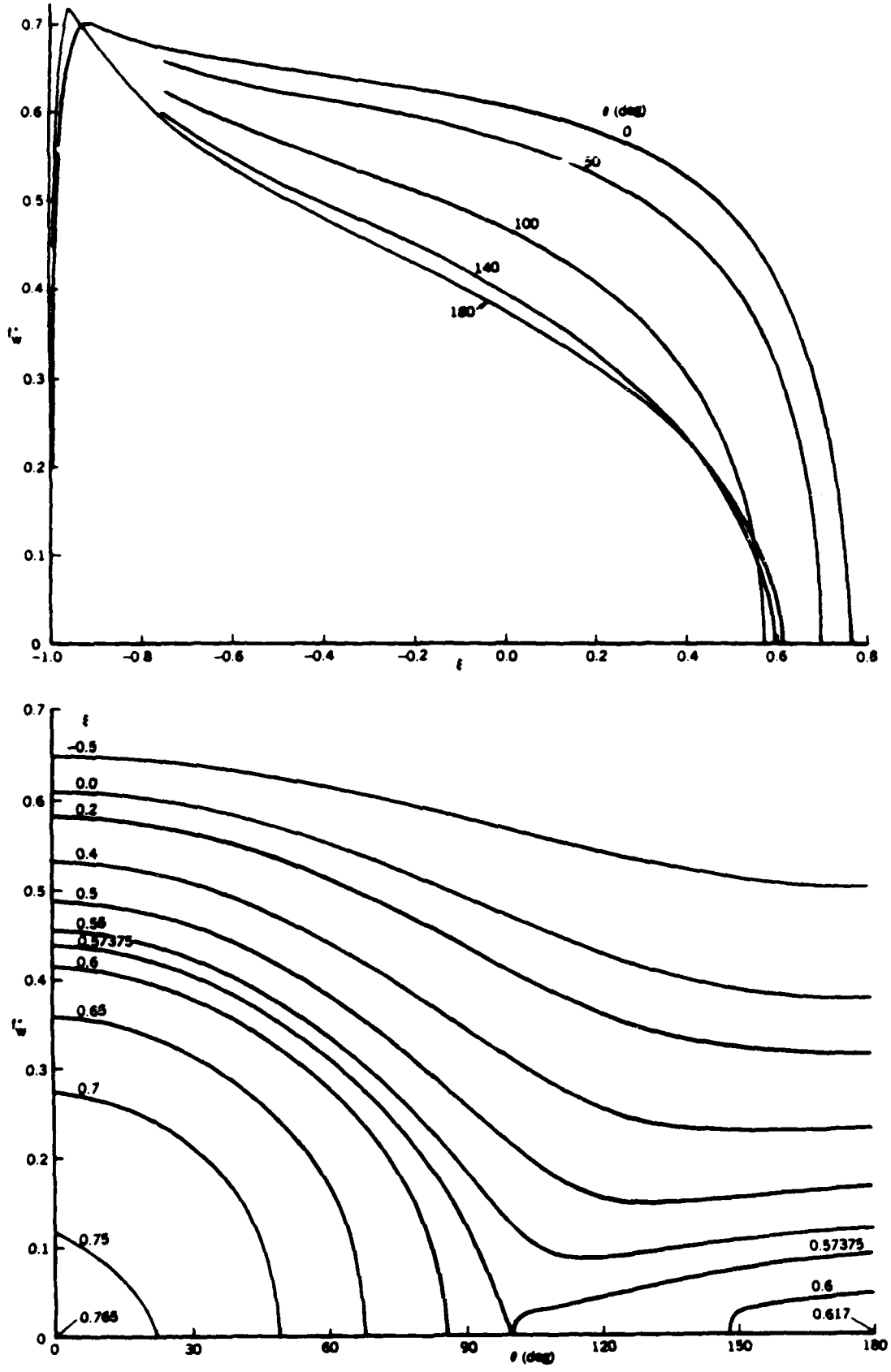

Figure 7. Variation of the streamwise wall shear f''_w with (a) ξ and (b) θ at different values of θ and ξ, respectively, for $\alpha = 3°$.

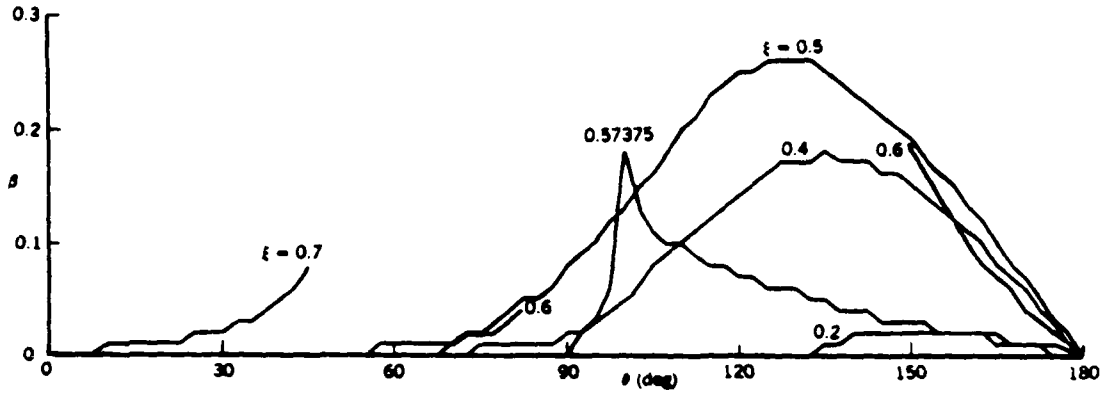

Figure 8. Variation of the stability parameter β with θ at general values of ξ for α = 3°.

Figure 9 shows the approximate direction field of the limiting streamlines g_w''/f_w'' (indicated by dashed lines) and the integrated trajectories (indicated by solid lines) in the θ - ξ plane. Figure 10 shows the limiting streamlines obtained by integrating the direction field of the wall shear $h_1 g_w''/h_2 f_w''$ as a function of ξ and θ plotted on the body. We note that the limiting streamlines which were parallel to the ξ-direction at α = 0 are now deflected from the ξ-direction due to the effect of the pressure gradient in the θ-direction. As in the case of α = 6°, the calculations lead to definitions of terminal lines 1 and 2 which correspond to the breakdown of the calculations due to the singular nature of the boundary-layer equations. In these regions, the slopes of the limiting streamlines change rapidly and approach ±90° as the solutions break down. It is clear from this figure and from Fig. 6, that the first point at ξ = 0.57375, θ = 100°, which corresponds to negative g_w'' and zero f_w'' can be regarded (as in the case of α = 6°) as the beginning of the separation line for α = 3° and can be used to identify the skin-friction line as the separation line in three-dimensional flows. The behavior of the skin-friction lines on both sides of the separation line is again similar to that for α = 6° discussed by Cebeci and Su (1988).

Figures 11 to 13 show the results for α = 2° and 1° and the first flow reversal in the circumferential flow direction takes place at ξ_A = 0.17 and

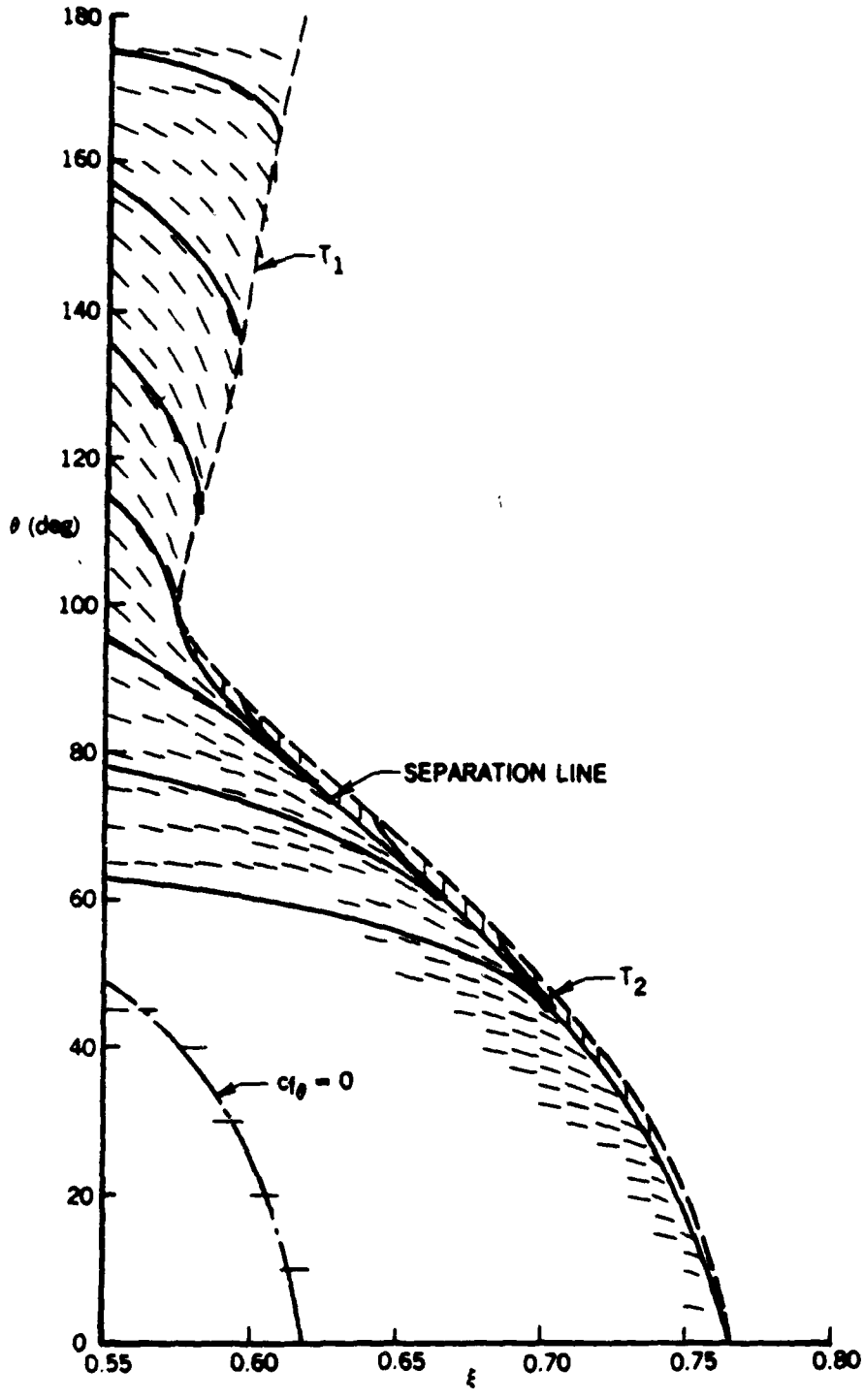

Figure 9. Approximate direction field of the limiting streamlines (dashed lines) and integrated trajectories (solid lines). The long dashed line SP denotes terminal line 1, PN terminal line 2, and the solid line PN the separation line.

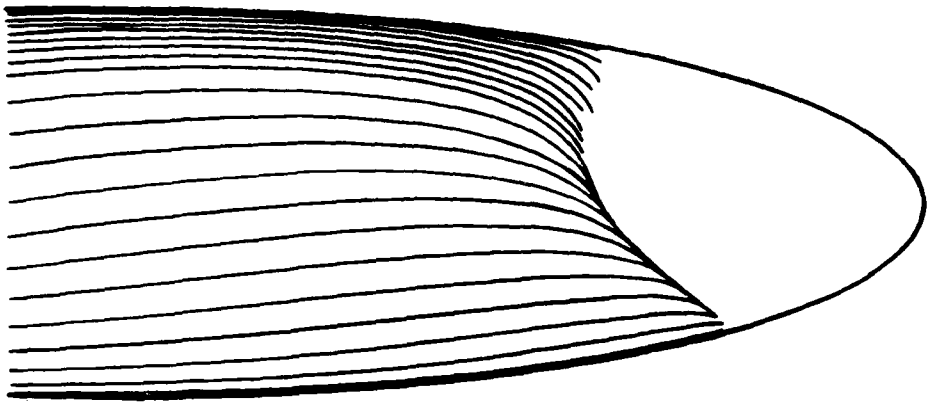

Figure 10. Behavior of the limiting streamlines on the body for $\alpha = 3°$.

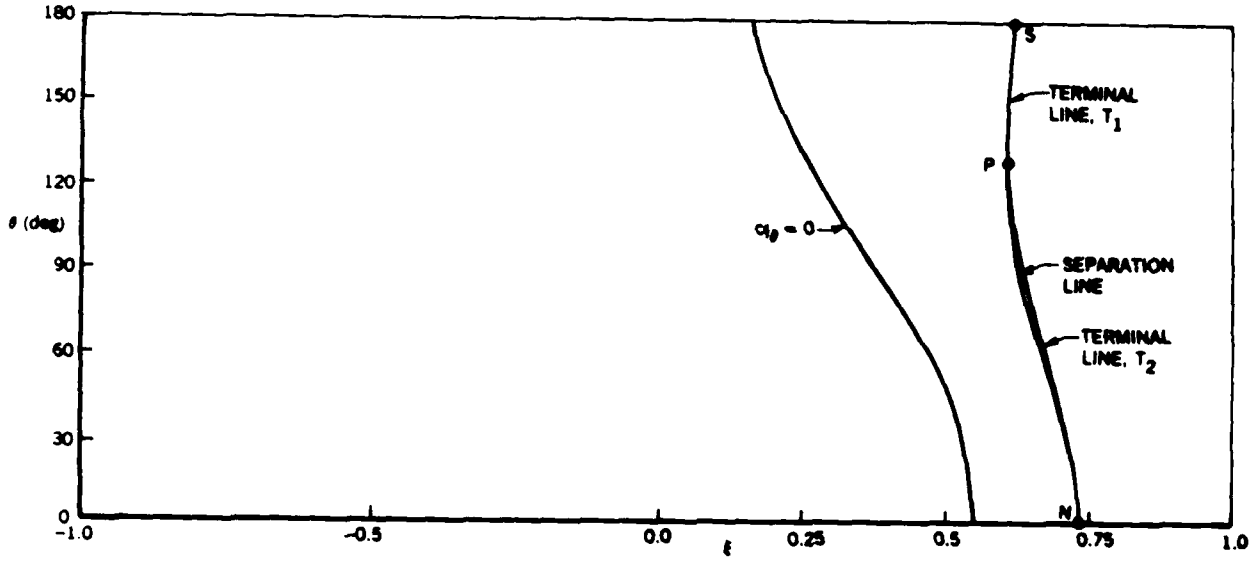

Figure 11. Flow regions for $\alpha = 2°$. ξ_S and ξ_N correspond to the separation locations on the leeward and windward sides, respectively.

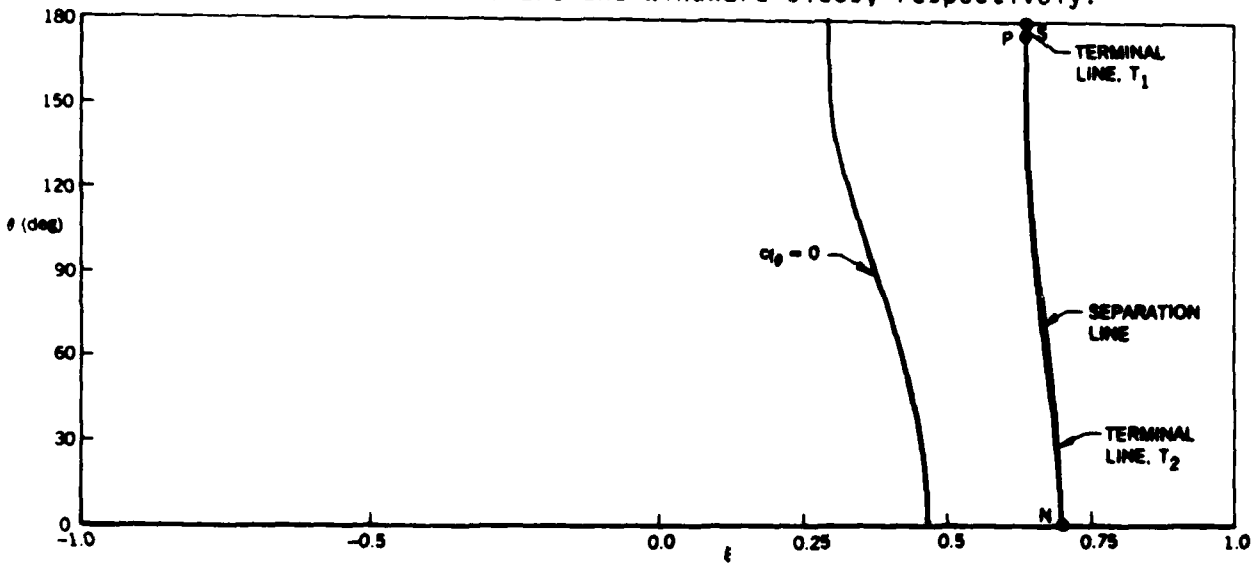

Figure 12. Flow regions for $\alpha = 1°$. ξ_S and ξ_N correspond to the separation locations on the leeward and windward sides, respectively.

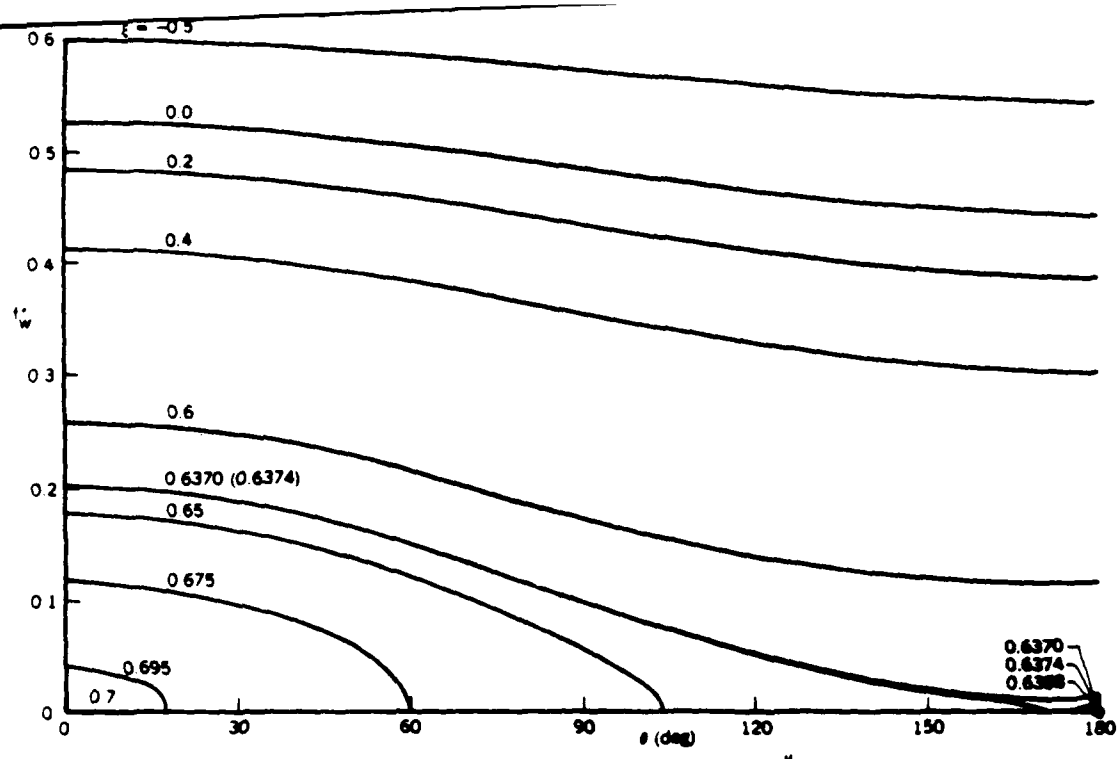

Figure 13. Variation of the streamwise wall shear f''_w with ξ at different values of θ for $\alpha = 1°$.

at $\xi_A = 0.290$, respectively. The first ξ-location where f''_w vanishes occurs at $\xi_p = 0.6098$, $\theta_p = 130°$ for $\alpha = 2°$, and at $\xi_p = 0.6374$, $\theta_p = 175°$ for $\alpha = 1°$. As for $\alpha = 3°$, the figures define two terminal lines and a separation line which is open and show that the beginning of the open separation line approaches the separation location on the leeward line of symmetry with increasing angle with open separation closed at $\alpha = 0$. Figure 13 shows the variation of the streamwise wall shear f''_w with θ at various ξ-locations on the body for $\alpha = 1°$ and that, as for $\alpha = 3°$ and the solutions are free of oscillations.

Figure 14 shows the open separation and $c_{f_\theta} = 0$ lines where the first flow reversal in the circumferential direction takes place at $\xi = -0.92$ on the leeward plane of symmetry, and where f''_w vanishes at $\xi = -0.8453$ at $\theta = 141.5°$ for $\alpha = 30°$. The calculations for this angle of attack were more difficult than those for $\alpha = 6°$ and it was necessary to use a nonuniform grid in both ξ and θ-directions, as shown in Tables 2 and 3. It is evident from Fig. 15 that the magnitude of β is relatively small for values of $\xi \leq -0.875$ and begins to increase sharply thereafter. For $\xi = -0.8453$, the magnitude of β reaches 0.57 at $\theta = 141.5°$ and it was possible calculate up to $\xi = -0.50$ in the second subregion. Overshoots in the velocity profiles (both in u and w) began to occur at $\xi = -0.50$ and became progressively worse. Refining the net did not help, and the calculations became very difficult to perform

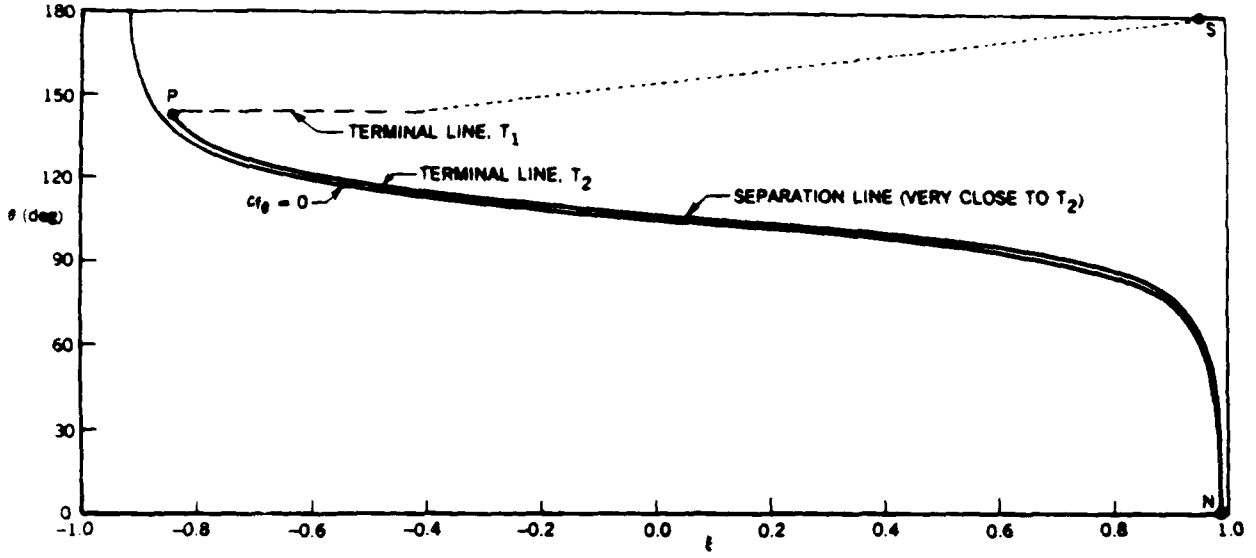

Figure 14. Flow regions for $\alpha = 30°$.

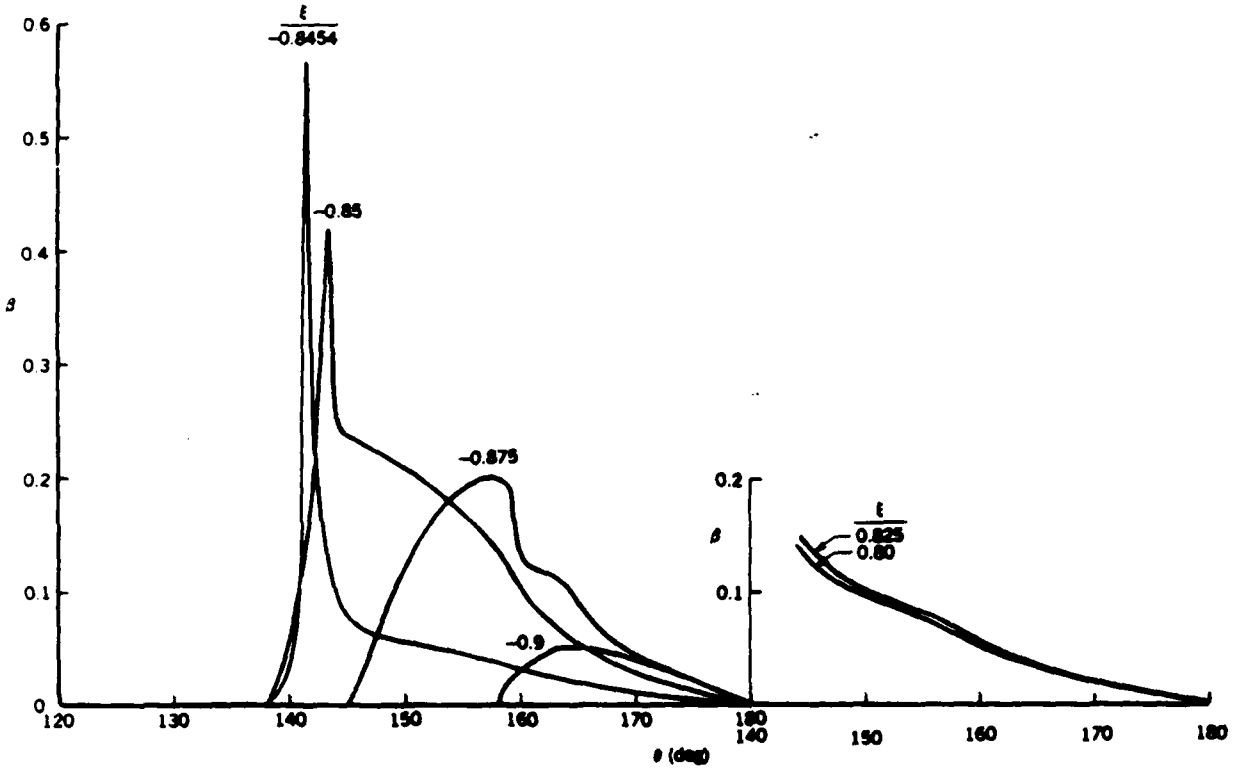

Figure 15. Variation of the stability parameter β with θ at several values of ξ for $\alpha = 30°$.

with increasing ξ where the circumferential edge velocity became bigger and the boundary-layer thicker. Figure 16 shows the variations of f_w'' with ξ and θ, for several values of θ and ξ, respectively, and indicates trends similar to those observed with $\alpha = 6°$. We note from Fig. 16a that f_w'' vanishes at $\xi_N = 0.988$ on the windward line of symmetry ($\theta = 0$), and at $\xi = 0.948$ on the

Table 2. Axial Step Length for $\alpha = 30°$

ξ	$\Delta\xi \times 10^2$
<-0.9	0.25
-0.9000 - -0.8640	0.10
-0.8640 - -0.8520	0.05
-0.8520 - -0.8500	0.04
-0.8500 - -0.8470	0.03
-0.8470 - -0.8456	0.02
-0.8456 - -0.8446	0.01
-0.8446 - -0.8418	0.02
-0.8410 - -0.7000	0.10
>-0.7000	0.20

Table 3. Circumferential Step Lengths for $\alpha = 30°$

$\xi < -0.8418$		$\xi > -0.8418$	
θ	$\Delta\theta$	θ	$\Delta\theta$
0° - 30°	5°	0° - 30°	5°
30° - 100°	2.5°	30° - 100°	2.5°
100° - 110°	2°	100° - 110°	2°
110° - 139°	1°	110° - 139°	1°
139° - 144°	0.5°	139° - 141°	0.5°
144° - 160°	1°	141° - 170°	3°
160° - 166°	1.5°	170° - 180°	5°
166° - 170°	2°		
170° - 180°	2.5°		

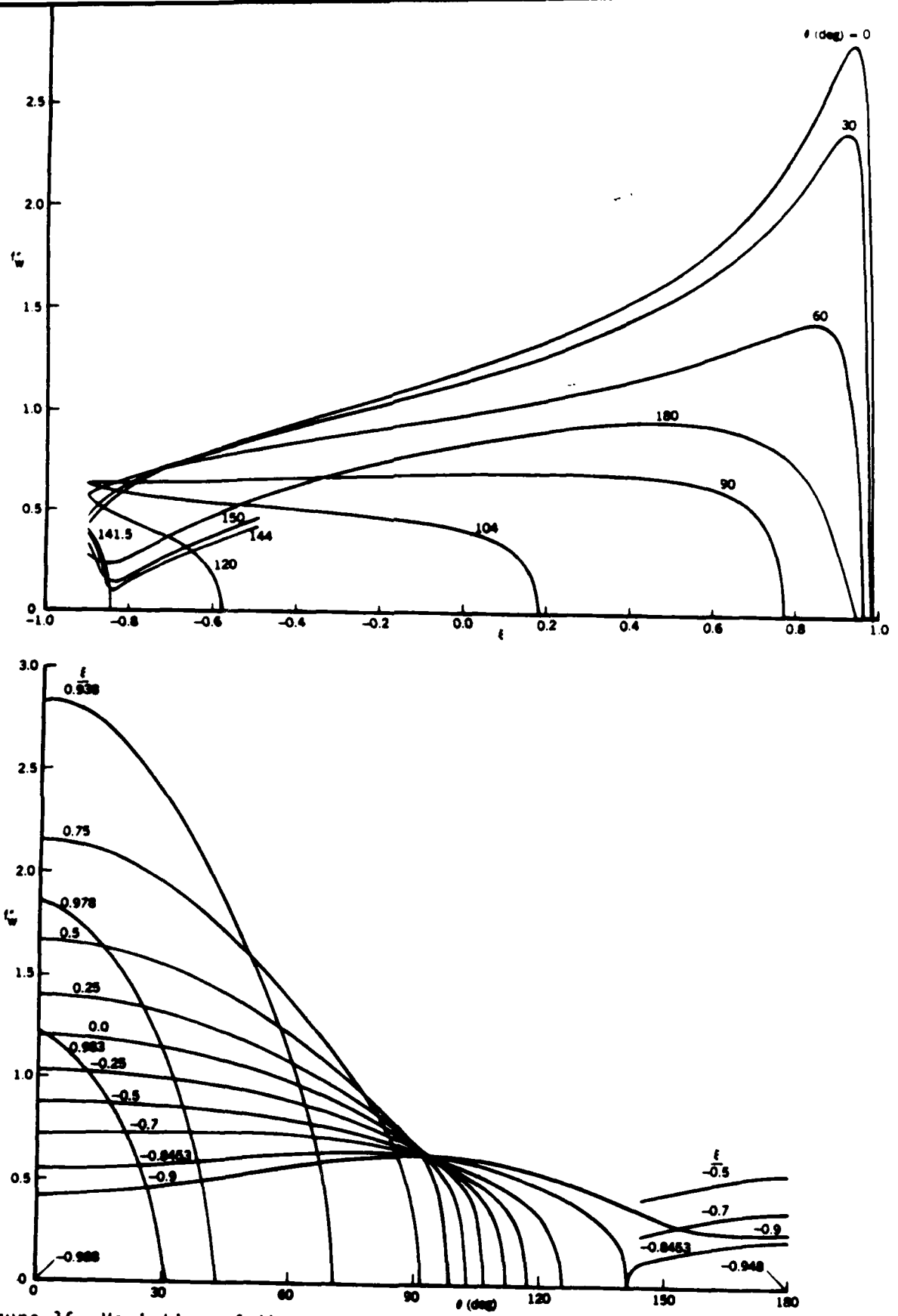

Figure 16. Variation of the streamwise wall shear with (a) ξ and (b) θ at different values of θ and ξ, respectively, for α = 30°.

leeward side. The first interior point where f''_w vanishes occurs at ξ_p = -0.8453 at θ_A = 141.5°. The variation of f''_w with θ for a given ξ-location, see Fig. 16b, shows that, the wall shear undergoes a drastic change near the region of flow separation, decreasing and increasing sharply at θ = 141.5° and this explains the need to employ a very fine grid in this region. In both figures, the behavior of f''_w is smooth and free of oscillations and indicates that the results are accurate and reliable.

Figure 17 shows the approximate direction field of the limiting streamlines (indicated by dashed lines), the integrated streamlines (indicated by solid lines), the c_{f_θ} = 0 line, separation line and terminal lines 1 and 2. There is clearly no problem in computing the flow in the third subregion after flow separation occurs at ξ = -0.8453 because the negative cross-flow region is very small. Consistent with the results for α = 1 to 3° and 6°, there is a separation line between the two lines representing c_{f_θ} = 0 and the terminal line 1. The approximate streamlines were obtained by integrating g''_w/f''_w as a function of ξ and θ with integration starting at ξ = -0.860 and their behavior is similar to those for α = 6°.

The separation lines of Fig. 18 may be compared with those of Figs. 2 to 4 with the clear implicaton that the present results agree well with the measurements of Meier et al. and, in the main, with those of Costis et al. The separation is open for all angles of attack greater than zero, at least for the prolate spheroid of fineness ratio six. It should be noted that the side view presented on Fig. 18 shows a small distance of open separation for angles of attack of 1, 2 and 3 degrees so that great care is likely to be required in the interpretation of near-surface visualization, as in the case of Costis et al.

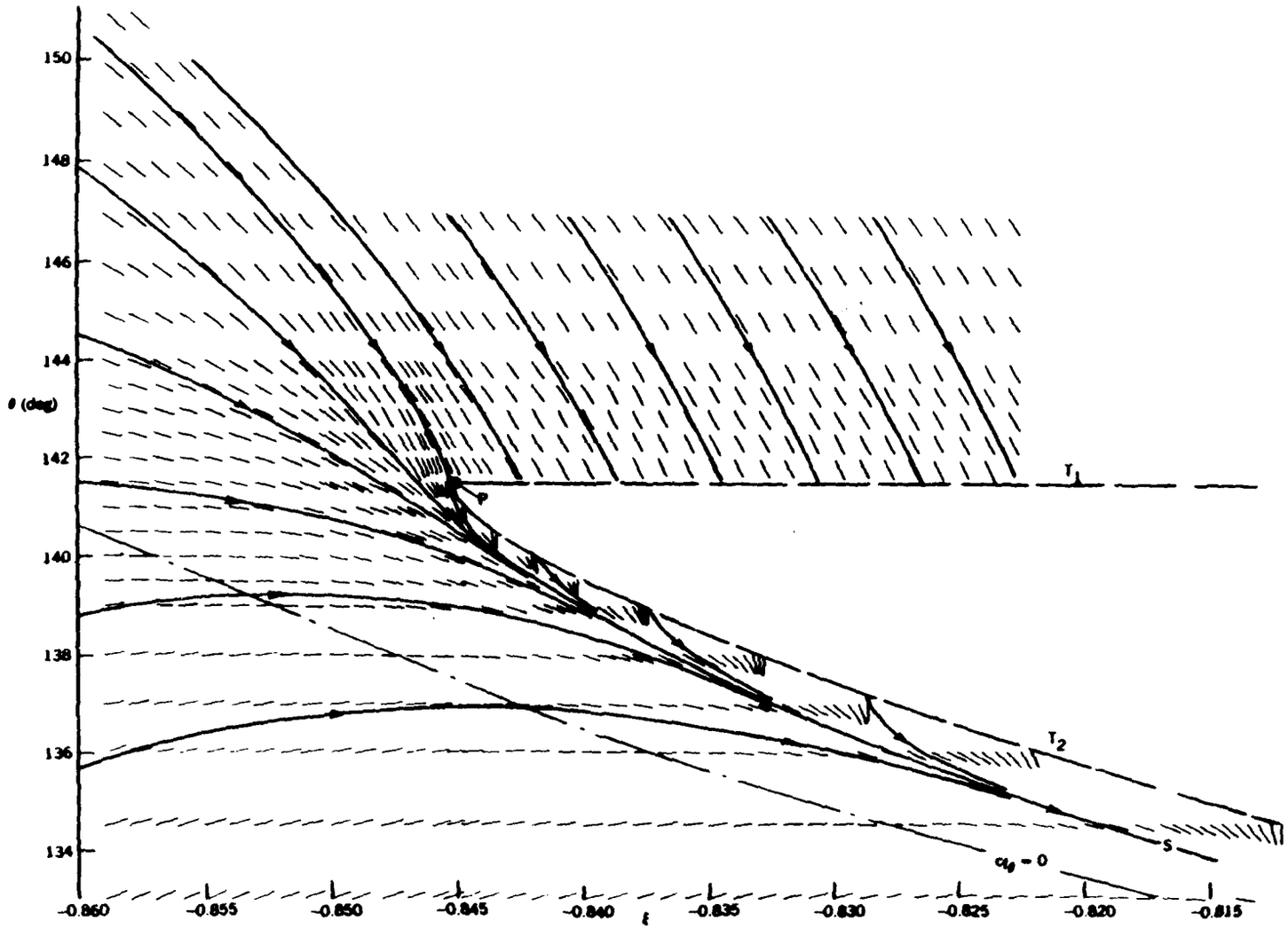

Figure 17. Approximate direction field of the limiting streamlines (dashed lines) and integrated streamlines (solid lines). The long dashed line Γ_1 denotes terminal line 1, Γ_2 terminal line 2 and the heavy solid line FS the separation line.

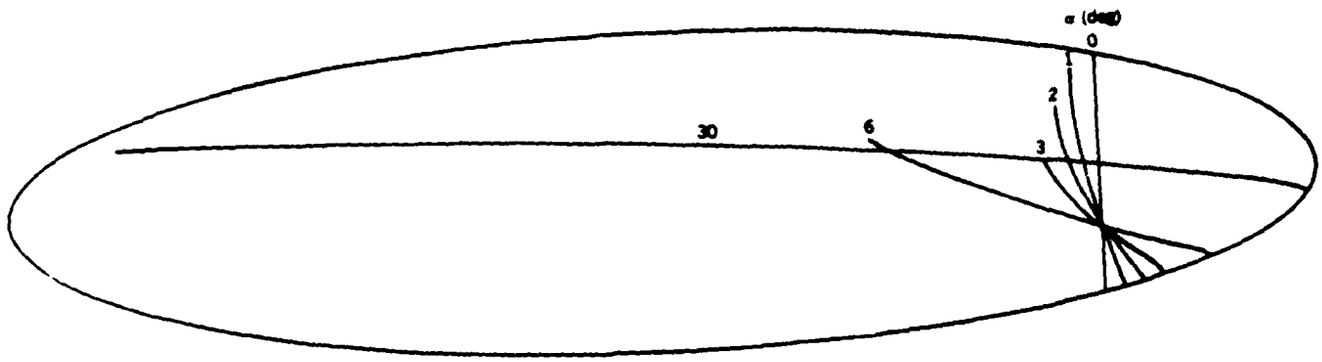

Figure 18. The separation lines on the prolate spheroid at various angles of attack.

4.0 CONCLUDING REMARKS

The results of the preceeding section confirm that separation is open for all angles of attack considered and described by a line which corresponds to a skin-friction line, as suggested by Lighthill. The lines of zero c_{f_θ} occur upstream of separation and terminal lines are identified beyond which the boundary-layer equations cannot be solved with a prescribed pressure distribution. It is evident that great care is required to ensure numerical accuracy and that this has been achieved by a combination of the standard and characteristic box methods with an essential stability criterion.

5.0 REFERENCES

Cebeci, T. and Su, W. 1988 Separation of Three-Dimensional Boundary Layers on a Prolate Spheroid. J. Fluid Mech. 191, pp. 47-77.

Cebeci, T., Khattab, A.A. and Stewartson, K. 1981 Three-Dimensional Laminar Boundary Layers and the Ok of Accessibility. J. Fluid Mech. 107, pp. 57-87.

Cebeci, T., Khattab, A.A. and Stewartson, K. 1980 On Nose Separation. J. Fluid Mech. 7, pp. 435-454.

Costis, C.E., Polen, D.M. Hoang, N.T. and Telionis, D.P. 1988 Laminar Separating Flow Over a Prolate Spheroid. To be published in J. Aircraft.

Han, T.Y. and Patel, V.C. 1979 Flow Separation on a Spheroid at Incidence. J. Fluid Mech. 92, pp. 643-657.

Lighthill, M.J. 1963 In Laminar Boundary Layers. (L. Rosenhead, ed) Chap. 2, p. 79, Oxford University Press.

Maskell, E.C. 1955 Flow Separation in Three Dimensions. Rep. Aero. Res. Coun. Lond. No. 18063.

Meier, H.U. and Kreplin, H.-P. 1980 Experimental Investigation of the Boundary-Layer Transition and Separation on a Body of Revolution. Z. Flugwiss, Weltraumforschung 4, Helft 2, pp. 65-71.

Meier, H.W., Kreplin, H.P. and Vollmers, H. 1983 Development of Boundary Layers and Separation Patterns on a Body of Revolution at Incidence. In Proceedings of Second Symposium on "Numerical and Physical Aspects of Aerodynamic Flows," California State University, Long Beach, 17-20 Jan.

Wang, K.C. 1975 Boundary Layer Over a Blunt Body at Low Incidence with Circumferential Reverse Flow. J. Fluid Mech. 72, pp. 49-65.

Wang, K.C. 1976 Separation of Three-Dimensional Flow. Proceedings of the Viscous Flow Symposium, held at Lockheed-Georgia Co., 22-23 June.

Williams, J.C. 1977 Incompressible Bounday-Layer Separation. J. Fluid Mech. 9, pp. 113-144.